Ferromagnetic resonance in thin films submitted to multiaxial stress state: application of the uniaxial equivalent stress concept and experimental validation

2016 J. Phys. D: Appl. Phys. 49 265001

(http://iopscience.iop.org/0022-3727/49/26/265001)

IOP Publishing Journal of Physics D: Applied Physics
J. Phys. D: Appl. Phys. **49** (2016) 265001 (7pp) doi:10.1088/0022-3727/49/26/265001

Ferromagnetic resonance in thin films submitted to multiaxial stress state: application of the uniaxial equivalent stress concept and experimental validation

M Gueye[1], F Zighem[1], M Belmeguenai[1], M Gabor[2], C Tiusan[2] and D Faurie[1]

[1] LSPM-CNRS, Université Paris XIII, Sorbonne Paris Cité, 93430 Villetaneuse, France
[2] Center for Superconductivity, Spintronics and Surface Science, Technical University of Cluj-Napoca, Str. Memorandumului No. 28 RO-400114, Cluj-Napoca, Romania

E-mail: zighem@univ-paris13.fr

Received 25 February 2016, revised 6 April 2016
Accepted for publication 21 April 2016
Published 26 May 2016

Abstract

In this paper a unique expression of the anisotropy field induced by any multiaxial stress state in a magnetic thin film and probed by ferromagnetic resonance is derived. This analytical development has been made using the uniaxial equivalent stress concept, for which correspondances between definitions given by different authors in the literature is found. The proposed model for the anisotropy field has been applied to Co_2FeAl thin films (25 nm) stressed both by piezoelectric actuation (non-equi-biaxial) or by bending tests (uniaxial) and measured with a broadband ferromagnetic resonance technique. The overall exprimental data can be easily plotted on a unique graph from which the magnetostriction coefficient has been estimated.

Keywords: ferromagnetic resonance, magnetoelasticity, thin films

(Some figures may appear in colour only in the online journal)

1. Introduction

The study of the magnetic properties of thin films subjected to deformations of various origins (electrical or mechanical) has grown considerably in recent years [1–6] for both potential application and fundamental reasons. One of the most prominent applications concerns the control of magnetization by an electric field in systems combining ferroelectric and ferromagnetic materials [7–10] (artificial multiferroics materials). On the other hand, the study of ferromagnetic films deposited on flexible substrate requires a thorough understanding of the effect of deformation on the functional properties [11–13]. Indeed, when they are deposited on polymer substrates (Kapton, PDMS, PET, ...) for applications in flexible spintronics, they can be subjected to high stresses which could affect their static magnetic configuration and propagation of spin waves. In many cases, the study of magnetoelastic properties of alloy thin films, sometimes still unclear, is inevitable for applying them to magnetoresistive sensors (GMR for example) [14, 15].

The effect of mechanical stress state, which can be of various origin (for instance bending strain [16, 17] or non-equi-biaxial strain induced by a piezoelectric substrate [18, 19]) should be studied carefully. In order to compare the effect resulting from different sollicitations, the simpliest way is to introduce the multiaxiality of the stress state into the classical uniaxial models through the definition of a fictive uniaxial stress: the equivalent stress that would change the magnetic behavior in a similar manner as the multiaxial one. Several attempts are available in the literature [20–23], where the most general definition of the equivalent uniaxial stress has been given by Daniel and Hubert in 2010 [24, 25].

A method that has proven to estimate the magnetoelastic behavior of ultra thin films (down to a few nanometers) is to combine mechanical testings and a broadband ferromagnetic resonance (FMR) in external magnetic field and study quantitatively the evolution of the resonance field and/or anisotropy field [26–29]. In this paper, we propose to use microstrip ferromagnetic resonance (MS-FMR) for studying in detail

the magnetoelastic properties of Co_2FeAl thin films (25 nm) grown on Kapton® submitted to strain induced by piezoelectric actuation (non-equi-biaxial) or by bending tests (uniaxial). After a comparison of results (study of the anisotropy field and determination of the magnetostriction coefficient) for these tests under applied magnetic field, we will show how the definition of the equivalent uniaxial stress allows plotting the whole data on a single graph.

2. Theoretical background: magnetoelastic effects probed by FMR

In this paragraph, the resonance field of the uniform precession mode of a magnetostrictive film submitted to in-plane external stresses is derived in the macrospin approximation (i.e. a uniform magnetization is considered).

2.1. Multiaxial stress and resulting anisotropy field

In our system, these in-plane stresses are applied either by a piezoelectric medium or by a curved support. For simplicity, the magnetostrictive and elastic properties of this thin film are considered as isotropic at the macroscopic scale (it will be the case in the studied system). With these assumptions (isotropic behavior and macrospin approximation), the magnetostriction coefficient, Young's modulus and Poisson's ratio of the thin film are scalar parameters. The magnetic energy of the thin film can be written as:

$$F = F_{zee} + F_{dip} + F_{me} \tag{1}$$

where the two first terms stand for the Zeeman and dipolar contributions, respectively. The last term corresponds to the magnetoelastic energy term for which the expression for a general stress state is [24]:

$$F_{me} = -\lambda\left[\frac{3}{2}{}^t\vec{\alpha}\underline{\underline{\sigma}}\vec{\alpha} - \frac{1}{2}\mathrm{tr}(\underline{\underline{\sigma}})\right] \tag{2}$$

where $\vec{\alpha} = (\cos\varphi_M \sin\theta_M, \sin\varphi_M \sin\theta_M, \cos\theta_M)$ is the unit vector along the magnetization and λ is defined as the isotropic magnetostriction coefficient at saturation of the thin film (see figure 1(a)). $\underline{\underline{\sigma}}$ is the stress tensor that has the following general form in the absence of shear stress:

$$\underline{\underline{\sigma}} = \begin{pmatrix} \sigma_{xx} & 0 & 0 \\ 0 & \sigma_{yy} & 0 \\ 0 & 0 & \sigma_{zz} \end{pmatrix} \tag{3}$$

where σ_{xx}, σ_{yy} and σ_{zz} are the orthogonal normal stresses.

Then, the magnetoelastic energy is:

$$F_{me} = -\frac{3}{2}\lambda(\sigma_{xx}\cos^2\phi_M \sin^2\theta_M + \sigma_{yy}\sin^2\phi_M \sin^2\theta_M + \sigma_{zz}\cos^2\theta_M) + \frac{\lambda}{2}(\sigma_{xx} + \sigma_{yy} + \sigma_{zz}) \tag{4}$$

The situation could be simplified if an in-plane magnetic field is applied (sufficiently strong to ensure a uniform magnetization distribution), the equilibrium polar angle is thus $\theta_M = \frac{\pi}{2}$ because of the large effective demagnetizing field

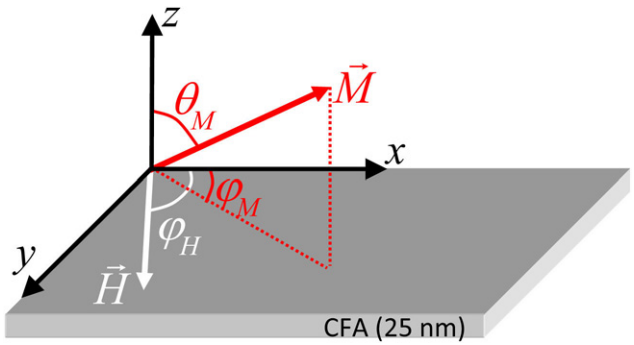

Figure 1. Schematic illustration showing the angles and the coordinate system used in the text.

associated with the planar film geometry, the magnetoelastic energy can finally be expressed as:

$$F_{me}\left(\theta_M = \frac{\pi}{2}\right) = -\frac{\lambda}{4}[\sigma_{xx}(1 + 3\cos 2\varphi_M) + \sigma_{yy}(1 - 3\cos 2\varphi_M) - 2\sigma_{zz}] \tag{5}$$

An equivalent stress σ_{eq}^{DH} has been introduced by Daniel and Hubert [24, 25] and comes from the general expression of the magnetoelastic energy in the isotropic case, e.g. from equation (2). It defines a fictive uniaxial stress that would change the magnetic behavior in a similar manner than a multiaxial one. This is particularly useful to compare results obtained from different kinds of sollicitations, as will be shown in this paper. Indeed, from equation (2), being given that the magnetoelastic energy for a given uniaxial stress $\sigma_{uniaxial}$ is $F_{me} = -\lambda\sigma_{uniaxial}$, the equivalent stress introduced by Daniel and Hubert can be expressed as follows:

$$\sigma_{eq}^{DH} = \frac{3}{2}{}^t\vec{\alpha}\underline{\underline{\sigma}}\vec{\alpha} - \frac{1}{2}tr(\underline{\underline{\sigma}}). \tag{6}$$

If we consider the specific 'in-plane' case ($\theta_M = \frac{\pi}{2}$), this equivalent stress becomes:

$$\sigma_{eq//}^{DH} = \frac{1}{4}[\sigma_{xx}(1 + 3\cos 2\varphi_M) + \sigma_{yy}(1 - 3\cos 2\varphi_M) - 2\sigma_{zz}]. \tag{7}$$

Moreover, from the energy (equation (4)), it is convenient to introduce an 'effective' magnetoelastic anisotropy field, where magnitude can be defined as follows for an in-plane magnetization:

$$H_{me}(\varphi_M) = \frac{1}{M_s}\frac{\partial^2 F_{me}}{\partial\phi_M^2}\bigg|_{\theta_M=\frac{\pi}{2}} = \frac{3\lambda(\sigma_{xx} - \sigma_{yy})\cos 2\varphi_M}{M_s}. \tag{8}$$

If one considers the x axis ($\varphi_M = 0$), we find the following expression for the magnetoelastic anisotropy field:

$$H_{me} = \frac{3\lambda(\sigma_{xx} - \sigma_{yy})}{M_s}. \tag{9}$$

This expression is independent of σ_{zz} and is directly related to the difference of stresses along the principal axes x and y.

We will discuss the links with the equivalent stress $\sigma^{DH}_{eq//}$ in the next section.

2.2. Resonance field as a function of equivalent uniaxial stress

The resonance field of the uniform precession mode evaluated at the equilibrium is obtained from the following expression [30]:

$$\left(\frac{2\pi f}{\gamma}\right)^2 = \left(\frac{1}{M_s \sin\theta_M}\right)^2 \left(\frac{\partial^2 F}{\partial\theta_M^2}\frac{\partial^2 F}{\partial\varphi_M^2} - \left(\frac{\partial^2 F}{\partial\theta_M \varphi_M}\right)^2\right) \quad (10)$$

where f is the microwave driving frequency, M_s is the saturation magnetization and γ is the gyromagnetic factor ($\gamma = g \times 8.794 \times 10^6\ s^{-1}\cdot Oe^{-1}$). The different energy derivatives are evaluated at the equilibrium direction of the magnetization. An explicit expression can be derived for an in-plane applied magnetic field ($\theta_M = \frac{\pi}{2}$):

$$\left(\frac{2\pi f}{\gamma}\right)^2 = \left[4\pi M_s + H_{res}\cos(\varphi_M - \varphi_H) + \frac{3\lambda}{M_s}(\sigma_{xx}\cos^2\varphi_M + \sigma_{yy}\sin^2\varphi_M - \sigma_{zz})\right] \times \left[H_{res}\cos(\varphi_M - \varphi_H) + \frac{3\lambda}{M_s}(\sigma_{xx} - \sigma_{yy})\cos 2\varphi_M\right]. \quad (11)$$

Here φ_H is the angle between the in-plane applied magnetic field and x direction (see figure 1(a)). The analysis can be simplified in the assumption of a magnetization aligned along the applied magnetic field ($\varphi_M \simeq \varphi_H$). From equation (11), the resonance field of the uniform mode can be expressed as:

$$H_{res}(\varphi_M \simeq \varphi_H) = \sqrt{(2\pi M_s)^2 + \left(\frac{2\pi f}{\gamma}\right)^2 + H_a H_b} - 2\pi M_s - \frac{3\lambda}{M_s}\sigma^{DH}_{eq//} \quad (12)$$

where

$$H_a = \frac{3\lambda}{2M_s}(\sigma_{xx}\sin^2\varphi_M + \sigma_{yy}\cos^2\varphi_M - \sigma_{zz}) \quad (13)$$

and

$$H_b = 4\pi M_s + \frac{3\lambda}{2M_s}(\sigma_{xx}\sin^2\varphi_M + \sigma_{yy}\cos^2\varphi_M - \sigma_{zz}). \quad (14)$$

Given that the order of the stress-induced anisotropy is twofold, it is convenient to determine the magnitude of the magnetoelastic anisotropy field by measuring the total amplitude of the angular dependance of the resonance field H_{res}. Here, we can introduce the FMR-magnetoelastic field determined by the following expression, and that can be measured from in-plane angular dependence of the resonance field [31]:

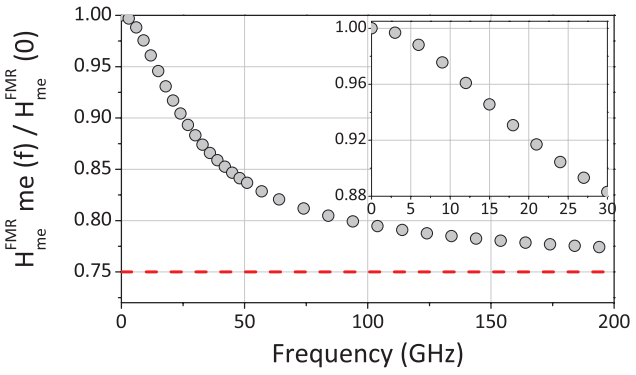

Figure 2. Frequency dependence of H^{FMR}_{me} for a large frequency range. The insert shows this frequency dependence for the usual FMR frequency range (0–30 GHz).

$$2H^{FMR}_{me} = \left[H_{res}(\varphi_M = \frac{\pi}{2}) - H_{res}(\varphi_M = 0)\right]. \quad (15)$$

This can be expressed as follows:

$$2H^{FMR}_{me} = \frac{9\lambda}{2M_s}(\sigma_{xx} - \sigma_{yy}) + \left[(2\pi M_s)^2 + \left(\frac{2\pi f}{\gamma}\right)^2 + 6\pi\lambda(\sigma_{xx} - \sigma_{zz}) + \left(\frac{3\lambda(\sigma_{xx} - \sigma_{zz})}{2M_s}\right)^2\right]^{1/2} - \left[(2\pi M_s)^2 + \left(\frac{2\pi f}{\gamma}\right)^2 + 6\pi\lambda(\sigma_{yy} - \sigma_{zz}) + \left(\frac{3\lambda(\sigma_{yy} - \sigma_{zz})}{2M_s}\right)^2\right]^{1/2}. \quad (16)$$

In each square-root of (16), with standard experimental conditions ($(\sigma_{xx} - \sigma_{zz})$ and $(\sigma_{yy} - \sigma_{zz})$ of the order of 100 MPa, $\lambda \sim 20 \times 10^{-6}$, $M \sim 1000$ emu $\cdot$ cm^{-3}, f of a few GHz, and $\frac{\gamma}{2\pi} = 0.003$ GHz $\cdot$ Oe^{-1}) the third term is about 3 orders of magnitude higher than the fourth one and 5 lower than the two first ones. Thus, concerning the two terms related to magnetoelastic contribution, the fourth term can be neglected as compared to the third one. Finally, the usual way is to apply the following first-order Taylor expansion inside each square-root (with $i = x, y$):

$$\left[(2\pi M_s)^2 + \left(\frac{2\pi f}{\gamma}\right)^2 + 6\pi\lambda(\sigma_{ii} - \sigma_{zz})\right]^{1/2} \approx \left((2\pi M_s)^2 + \left(\frac{2\pi f}{\gamma}\right)^2\right)^{\frac{1}{2}}\left(1 + \frac{1}{2}\frac{6\pi\lambda(\sigma_{ii} - \sigma_{zz})}{(2\pi M_s)^2 + \left(\frac{2\pi f}{\gamma}\right)^2}\right). \quad (17)$$

Therefore, the magnetoelastic anisotropy can be expressed as:

$$H^{FMR}_{me} \approx \frac{9\lambda}{4M_s}(\sigma_{xx} - \sigma_{yy}) + \frac{3\pi\lambda(\sigma_{xx} - \sigma_{yy})}{2\sqrt{(2\pi M_s)^2 + \left(\frac{2\pi f}{\gamma}\right)^2}}. \quad (18)$$

One can note that H^{FMR}_{me} depends on the frequency, this variation being shown on figure 2 ($H^{FMR}_{me}(f)$)/($H^{FMR}_{me}(f = 0)$) as a function of f. At $f = 0$ GHz, the FMR resonance field is equal to the static one H_{me} already determined in equation (9).

It decreases with frequency, according to equation (18), and gradually approaches $\frac{3}{4}H_{me}$.

In our standard range (0–10 GHz), one can see that H_{me}^{FMR} is very close to H_{me} so that the expression can be rewritten as:

$$H_{me}^{FMR}(f) \approx H_{me} \approx \frac{3\lambda}{M_s}(\sigma_{xx} - \sigma_{yy}). \quad (19)$$

Concerning the stress dependance, this expression suggests that in the case of an in-plane magnetized thin film, any given multiaxial stress state leads to an in-plane anisotropy field proportional to the term $(\sigma_{xx} - \sigma_{yy})$. This is consistent with the equivalent stress $\sigma_{eq}^{SR} = (\sigma_{xx} - \sigma_{yy})$ proposed by Schneider and Richardson [20] to describe the evolution of the anisotropy field with an applied biaxial stress state. Moreover, one can note that σ_{eq}^{SR} is simply equal to:

$$\sigma_{eq}^{SR} = -\frac{2}{3}\left[\sigma_{eq//}^{DH}\left(\varphi_M = \frac{\pi}{2}\right) - \sigma_{eq//}^{DH}(\varphi_M = 0)\right]. \quad (20)$$

Hence, the whole experimental data resulting from various kinds of solicitations (uniaxial or multiaxial) can be ploted in a common graph with the term $(\sigma_{xx} - \sigma_{yy})$ defining the abscissa axis and H_{me} the ordinate ones, as we will see in section 4.

3. Flexible system description and mastering the in-plane stresses

A 25 nm-thick Co_2FeAl film was first grown on a Kapton® substrate (of thickness 125 μm) using a magnetron sputtering system at room temperature and then capped with a Ta (5 nm) layer. Therefore, the film/substrate system can be cemented onto a piezoelectric actuator or onto a curved support. These two kinds of supports allow deforming the thin film, as described in the following. The structural properties of the as-deposited sample have been characterized by x-ray diffraction using a four-circle diffractometer. The x-ray $\theta - 2\theta$ diffraction pattern with diffraction vector $\vec{k}$ perpendicular to the surface revealed CFA peaks without preferential orientation (random polycrystal). Given this grain orientation distribution, we can estimate an in-plane Young's modulus $E = 263 \times 10^{10}$ dyn $\cdot$ cm^{-2} ($\equiv$ 263 GPa) and $\nu = 0.27$ from single-crystal elastic constants ($C_{11} = 253$ GPa, $C_{12} = 165$ GPa, $C_{44} = 153$ GPa [32]) by suitable averaging (homogenization method detailed by Faurie *et al* [33]).

Deformation in thin film may be applied either by a piezoelectric actuator or by bending. In the first method, we apply a voltage to the actuator which has the effect of straining it. The deformations are perfectly transmitted through interfaces (actuator/Kapton) and (Kapton/thin film) as shown in Zighem *et al* [34] and Gueye *et al* [35].

Figures 3(a) and (b) show the deformations measured by digital image correlation (DIC) as a function of the applied voltage. When applying a voltage, the mean values of ε_{xx} and ε_{yy} vary with $\frac{\varepsilon_{yy}}{\varepsilon_{xx}} \sim -0.625$, while the in-plane shear strain ε_{xy} remains unchanged (not shown here). In figure 3(a), the curve corresponds to a simple electric loading-unloading (0 V–200 V–0 V); the non-linearity characterized by a 'loop' shape is due to the

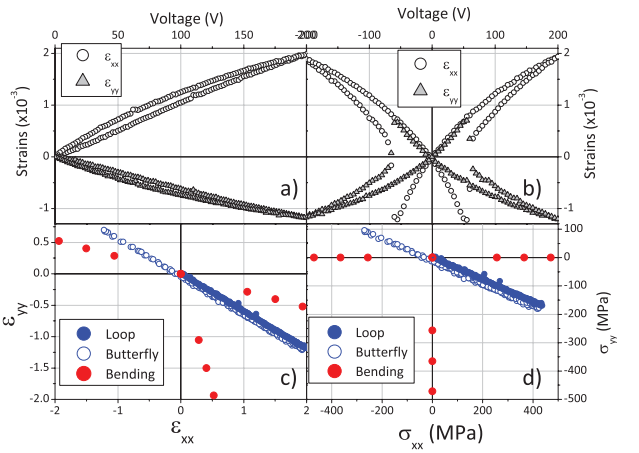

Figure 3. (a) ε_{xx} and ε_{yy} as a function of voltage applied to the piezoelectric actuator, measured by DIC, for a simple electric loading–unloading. (b) ε_{xx} and ε_{yy} as a function of voltage applied to the piezoelectric actuator, measured by DIC, for a symetric electric loading path. (c) ε_{yy} as a function of ε_{xx} for piezoelectric actuation ('loop' and 'butterfly' behavior) and unaxial bending. (d) σ_{yy} as a function of σ_{xx} for piezoelectric actuation ('loop' and 'butterfly' behavior) and unaxial bending.

specific piezoelectric behavior of the actuator, which is reversible. In figure 3(b), we show a symetrical cyclic loading path, i.e. an unloading from 200 to −200 V and a subsequent loading from −200 to 200 V. We observe the so-called 'butterfly' behavior that is due to polarization switching at about −60 V during unloading and 60 V during loading. Data shown in figures 3(a) and (b) are reported in a ε_{yy} *versus* ε_{xx} graph (figure 3(c)). The 'loop' (full blue circle symbols) and 'butterfly' (open blue symbols) data are well superimposed despite the polarization switching occuring in the case of cyclic path. From the values of ε_{xx} and ε_{yy}, it is straightforward to calculate the planar stresses σ_{xx} and σ_{yy} using isotropic Hooke's law, knowing the elastic constants of the polycrystalline film, given the isotropic crystallographic texture. The mean values of σ_{xx} and σ_{yy} vary with $\frac{\sigma_{yy}}{\sigma_{xx}} \sim -0.394$ as shown in figure 3(d).

In addition, we have also shown in figures 3(c) and (d) attainable strains and stresses respectively by bending the samples. These experiments have been performed by gluing the films onto small pieces of aluminium blocks of circular cross-section of known radii R: 32.2, 41.6, 59.2 mm and infinite (flat surface). More details about the *in situ* can be found in [14] and [36]. Here, the curvature stress can be applied either along the x axis or the y axis. When the bending is applied along the x axis, assuming that the film thickness is very small with respect to the substrate ones, the strains are given by:

$$\varepsilon_{xx} = \frac{t}{2R} \quad (21)$$

and

$$\varepsilon_{yy} = -\nu\frac{t}{2R} \quad (22)$$

where t is the whole sample thickness (∼the substrate thickness in our case) E is the film Young's modulus and ν the film Poisson's ratio.

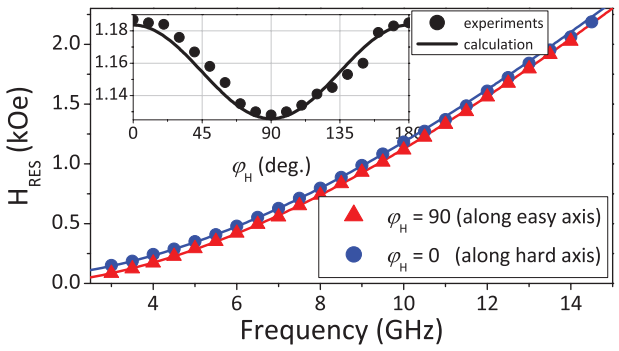

Figure 4. Evolution of the uniform mode resonance field H_{res} as a function of the microwave driven frequency f. Red triangular and black circled symbols refer for applied magnetic field along the easy ($\varphi_H = \frac{\pi}{2}$) and the hard ($\varphi_H = 0$) axes. The inset shows the in-plane angular dependance of the resonance field at $f = 10$ GHz. The solid lines are best fits of experimental data using the model decribed in the text. φ_H is the angle between the applied field and the x axis (one substrate edge).

In the case of bending along the y axis, the expressions of ε_{xx} and ε_{yy} are found by substituting one for the other. In any case, the uniaxial stress along the x axis or the y axis is found by using Hooke's law. In our conditions, the above-mentioned radii values correspond respectively to the following values of applied stresses : 0.47, 0.37, 0.26, 0 GPa. Moreover, the stress in the thin film is compressive if the film is in contact of the the bended-block and tensile if the substrate is the bended-block. We have thus studied three opposite stress states and the zero stress state (unbended sample).

4. Results and discussion

4.1. Magnetic characterization at zero stress

The MS-FMR measurements were carried out using field sweep in extended range at a fixed microwave excitation frequency as it is often the case in conventional FMR, usually called sweep field FMR [37]. Indeed, this method has been employed in order to probe the resonance field evolution versus the strains applied to the thin film. However, to determine some magnetic properties, such as the anisotropy constant and the gyromagnetic ratio, a beforehand characterization of the sample has been performed with zero applied voltage. Thus, the figure 4 shows the evolution of the uniform precession mode resonance field versus the microwave driven frequency for applied magnetic fields along the easy axis (corresponding to the y axis) and hard axis (x axis). The corresponding in-plane angular dependance of this resonance field, illustrated in figure 4 for 10 GHz driven frequency, is governed by a slight uniaxial anisotropy of 30 Oe, as deduced from the fit (solid lines in figure 4) assuming a planar configuration of the magnetization (viz. $\theta = \frac{\pi}{2}$). This in-plane anisotropy is generally attributed to a non equi-biaxial stress state induced by a slight curvature of the whole system [35].

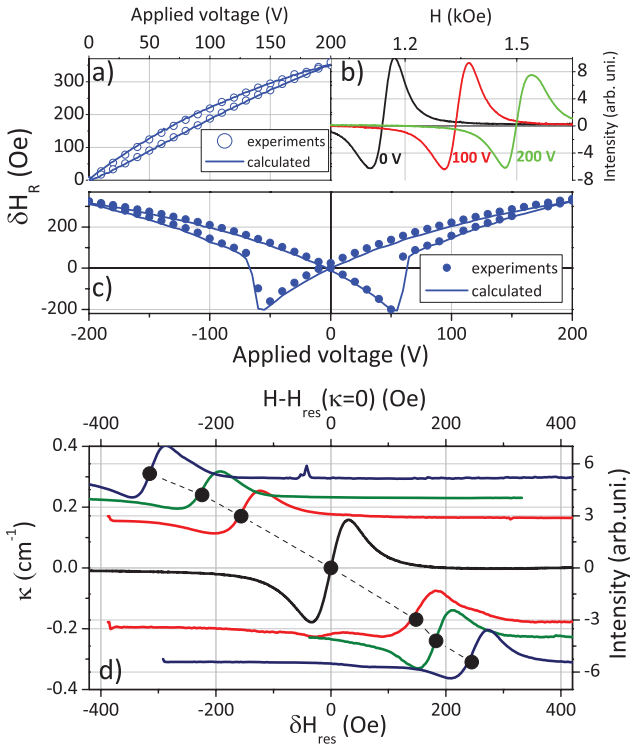

Figure 5. (a) Resonance field shift, defined as $\delta H_R = H_R(V) - H_R(V = 0)$, as a function of applied voltage to the piezoelectric actuator in the case of backward and forward voltage loops (0; 200 V). Circled points refer to experimental data while the solid line is the fit using the model described in equation (12). (b) Typical FMR spectra for different applied voltages (0 V, 100 V and 200 V). The positive shift is coherent with a positive magnetostriction coefficient of CFA. (c) Resonance field shift as a function of applied voltage to the piezoelectric actuator in the case of cyclic electric loading (−200; 200 V). (d) FMR spectra for bended samples with different curvatures $\kappa = \pm 1/R$ (here along the x axis). Circle symbols show the curvature κ as a function of $\delta H_R = H_R(\kappa) - H_R(\kappa = 0)$.

4.2. Confrontation of piezo-actuation and bending strain effects

In this section, we first study the influence of voltage-induced strains on the magnetization uniform precession mode by *in situ* MS-FMR measurements, before comparing these tests with bending ones. For this, the MS-FMR spectra have been recorded at 10 GHz microwave frequency and the magnetic static applied field has been varied. Backward and forward voltage loops (0–200 V) with steps of 10 V were applied to the PZT-actuator. The relative evolution of resonance field, defined as $\delta H_R = H_R(V) - H_R(V = 0)$, is shown in figure 5(a). Figure 5(b) shows the typical MS-FMR spectra at different applied voltages (0 V, 100 V and 200 V). Obviously, the resonance field evolution versus the voltage depends on the sign of the magnetostriction coefficient at saturation. For instance, Zighem *et al* [38] had shown left (negative) shift of the resonance field of uniform precession mode for an increasing applied voltage, for a Ni film with a negative magnetostriction coefficient at saturation $\lambda_{Ni} = -26 \times 10^{-6}$. Here, the positive shift of the resonance field suggests that polycrystalline CFA film has a positive effective magnetostriction coefficient, as shown in figures 5(a) and (b). Since the magnetoelastic field

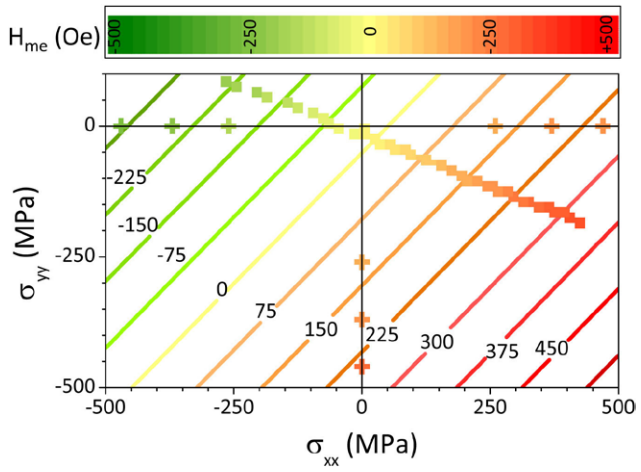

Figure 6. Theoretical (iso-anisotropy field lines) and experimental (square symbols for piezoactuation experiments, circle symbols for bending experiments) anisotropy field H_{me} map in the principal stress space (σ_{xx}, σ_{yy}).

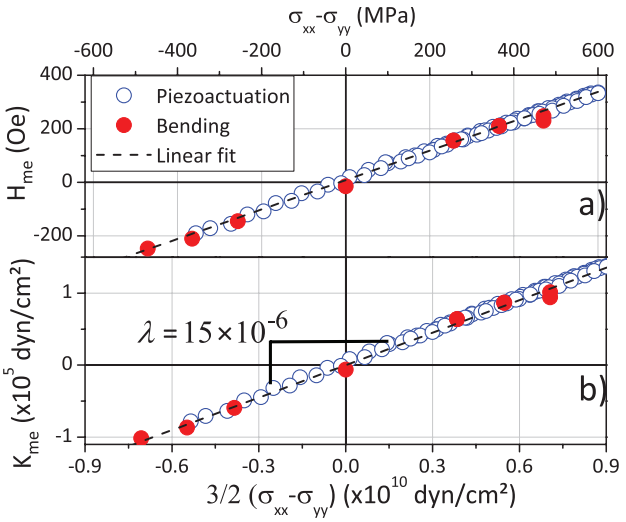

Figure 7. (a) Anisotropy field H_{me} as a function of $(\sigma_{xx} - \sigma_{yy})$. (b) Anisotropy constant K_{me}, as a function of $\frac{3}{2}(\sigma_{xx} - \sigma_{yy})$; knowing the magnetization at saturation, the slope of the linear regression directly gives the magnetostriction coefficient λ.

H_{me} is a voltage-dependent field, expressing the resonance field as a function of the applied voltage is equivalent to expressing the resonance field versus H_{me}. Thus, as shown on figure 5(a), a non-linear and loop-like behavior of the evolution of the uniform precession mode resonance field with the applied voltage and the magnetoelastic field is observed. As ferromagnetic films follow perfectly the elastic strains of the piezoelectric actuator, the hysteretic behavior of the resonance field shift can be explained by the intrinsic behavior (ferroelectric) of the actuator [38]. Moreover, this is confirmed by measurements made for the cyclic electric loading (figure 5(c)) for which we find a resonance field following perfectly the 'butterfly' behavior found in figure 3(c). All these experimental observations are well described by the theoretical model already described in Zighem *et al* [27].

Considering samples submitted to mechanical bending, figure 5(d) shows the evolution of MS-FMR spectra for different curvatures $\kappa = \pm 1/R$ along the x axis. The shift of the resonance field is related to the resulting applied uniaxial stresses given in figure 3(d). Obviously, this behavior is similar when the experiments are made along the y axis. In figure 6, we show the theoretical (iso-anisotropy field lines) and the experimental (square symbols for piezoactuation experiments, circle symbols for bending experiments) anisotropy field H_{me} mapped in the principal stress space (σ_{xx}, σ_{yy}). The analytical expression of $H_{me} = \left[H_{res}(\varphi_M = \frac{\pi}{2}) - H_{res}(\varphi_M = 0)\right]/2$ is given in equation (16) and is directly proportional to $(\sigma_{xx} - \sigma_{yy})$; that is why the iso-anisotropy field are perfectly linear. Here, the only fitting parameter is the magnetostriction coefficient $\lambda_{CFA} = 15 \times 10^{-6}$ (by fitting the overall data, very close to value previously found [14]) while saturation magnetization $M_S = 820$ emu $\cdot$ cm^{-3} has been measured by vibrating sample magnetometry. The accordance between model and experimental data seems very good and show that an equibiaxial stress state with opposite components favorizes the in-plane anisotropy.

However, from this map, it is not straightforward to compare the two kinds of experiments since one is biaxial and the other uniaxial. That is why we have plotted H_{me} as a function of $\sigma_{eq}^{DH}(\varphi_M = 0) - \sigma_{eq}^{DH}\left(\varphi_M = \frac{\pi}{2}\right) = \frac{3}{2}(\sigma_{xx} - \sigma_{yy})$ in order to underscore the efficiency of the equivalent stress concept, especially here for very thin films submitted to different sollicitations (figure 7(a)). We show here that the overall data (blue circle symbols for piezoactuation and red square symbols for bending) follows the same line on this graph. Obviously, a simple linear fit given by equation (16) allows determining the magnetostriction coefficient $\lambda_{CFA} = 15 \times 10^{-6}$, in a very simple and direct manner, as shown on figure 7 that presents $K_{me} = \frac{H_{me}M_s}{2}$ as a function of $\frac{3}{2}(\sigma_{xx} - \sigma_{yy})$. This good agreement between the voltage and the bending induced strain is another indication of the perfect strain transmission from the piezoelectric actuator to the CFA film.

5. Conclusion

We have derivated analytical solution of resonance field H_{res} and anisotropy field H_{me} in a magnetic film measured by FMR, for multiaxial stress state using the general uniaxial equivalent stress σ_{eq}^{DH} proposed by Daniel & Hubert [24]. Considering magnetization in the film plane due to demagnetizing field, the calculation leads to a very simple expression of H_{me} independant of σ_{zz}. As proposed by Schneider & Richardson [20] for a biaxial stress state, this expression is related to $(\sigma_{xx} - \sigma_{yy})$. However, this term resulting from σ_{eq}^{DH} cannot be viewed as an equivalent stress since it appears only in the specific expression of anisotropy field H_{me} (not in the resonance field H_{res} that is more substantial). This approach has been experimentally validated for a very thin film (Co_2FeAl) submitted to different sollicitations (uniaxial, non-equi-biaxial). Noticeably, we have shown that plotting K_{me} as a function of $\frac{3}{2}(\sigma_{xx} - \sigma_{yy})$, independently of the stress state, leads to a simple linear relationship englobing the whole experimental

data and allows determining the magnetostriction coefficient $\lambda_{CFA} = 15 \times 10^{-6}$. This method is valid for any magnetic thin film or nanostructures submitted to a multiaxial stress state.

References

[1] Finizio S *et al* 2014 *Phys. Rev. Appl.* **1** 021001
[2] Hu J-M, Li Z, Chen L-Q and Nan C-W 2012 *Adv. Mater.* **24** 2869
[3] Lei N *et al* 2013 *Nat. Commun.* **4** 1378
[4] Chopdekar R V *et al* 2012 *Phys. Rev.* B **86** 014408
[5] Zheng M *et al* 2014 *Phys. Rev.* B **90** 224420
[6] Singh S, Fitzsimmons M R, Lookman T, Jeen H and Biswas A 2014 *Phys. Rev.* B **90** 060407
[7] Shepley P M, Rushforth A W, Wang M, Burnell G and Moore T A 2014 *Sci. Rep.* **5** 7921
[8] Wang J J, Hu J M, Ma J, Zhang J X, Chen L Q and Nan C W 2014 *Sci. Rep.* **4** 7507
[9] Tkach A, Baghaie Yazdi M, Foerster M, Büttner F, Vafaee M, Fries M and Kläui M 2015 *Phys. Rev.* B **91** 024405
[10] Buzzi M, Chopdekar R V, Hockel J L, Bur A, Wu T, Pilet N, Warnicke P, Carman G P, Heyderman L J and Nolting F 2013 *Phys. Rev. Lett.* **111** 027204
[11] Melzer M, Makarov D, Calvimontes A, Karnaushenko D, Baunack S, Kaltofen R, Mei Y and Schmidt O G 2011 *Nano Lett.* **11** 2522
[12] Sun X, Bedoya-Pinto A, Llopis R, Casanova F and Hueso L E 2014 *Appl. Phys. Lett.* **105** 083302
[13] Yu Y *et al* 2015 *Appl. Phys. Lett.* **106** 162405
[14] Gueye M, Wague B M, Zighem F, Belmeguenai M, Gabor M S, Petrisor T, Tiusan C, Mercone S and Faurie D 2014 *Appl. Phys. Lett.* **105** 062409
[15] Páréz N, Melzer M, Makarov D, Ueberschär O, Ecke R, Schulz S E and Schmidt O G 2015 *Appl. Phys. Lett.* **106** 153501
[16] Singh S, Fitzsimmons M R, Lookman T, Jeen H, Biswas A, Roldan M A and Varela M 2012 *Phys. Rev.* B **85** 214440
[17] Magnus F, Moubah R, Kapaklis V, Andersson G and Hjörvarsson B 2014 *Phys. Rev.* B **89** 134414
[18] Heidler J, Piamonteze C, Chopdekar R V, Uribe-Laverde M A, Alberca A, Buzzi M, Uldry A, Delley B, Bernhard C and Nolting F 2015 *Phys. Rev.* B **91** 024406
[19] Wang Z, Zhang Y, Viswan R, Li Y, Luo H, Li J and Viehland D 2014 *Phys. Rev.* B **89** 035118
[20] Schneider C S and Richardson J M 1982 *J. Appl. Phys.* **53** 8136
[21] Kashiwaya K 1991 *Japan. J. Appl. Phys.* **30** 2932
[22] Sablik M J, Riley L, Burkhardt G, Kwun H, Cannel P, Watts K and Langman R 1994 *J. Appl. Phys.* **75** 5673
[23] Pearson J, Squire P T, Maylin M G and Gore J G 2000 *IEEE Trans. Magn.* **36** 3251
[24] Daniel L and Hubert O 2009 *J. Appl. Phys.* **105** 07A313
[25] Daniel L and Hubert O 2010 *IEEE Trans. Magn.* **46** 3089–92
[26] Li S, Xue Q, Duh J G, Du H, Xu J, Wan Y, Li Q and Lü Y 2014 *Sci. Rep.* **4** 7393
[27] Zighem F, Belmeguenai M, Faurie D, Haddadi H and Moulin J 2014 *Rev. Sci. Instrum.* **85** 103905
[28] Nesteruk K, Żuberek R, Piechota S, Gutowski M W and Szymczak H 2014 *Meas. Sci. Technol.* **25** 075502
[29] Jia C, Wang F, Jiang C, Berakdar J and Xue D 2015 *Sci. Rep.* **5** 11111
[30] Smit J and Beljers H G 1955 *Philips Res. Rep.* **10** 113
[31] Mc Michael R D, Stiles M D, Chen P J and Egelhoff W F Jr 1998 *Phys. Rev.* B **58** 9605
[32] Gabor M S, Petrisor T Jr, Tiusan C, Hehn M and Petrisor T 2011 *Phys. Rev.* B **84** 134413
[33] Faurie D, Djemia P, Le Bourhis E, Renault P-O, Roussigné Y, Chérif S M, Brenner R, Castelnau O, Patriarche G and Goudeau Ph 2010 *Acta Mater.* **58** 4998–5008
[34] Zighem F, El Bahoui A, Moulin J, Faurie D, Belmeguenai M, Mercone S and Haddadi H 2014 *J. Appl. Phys.* **116** 123903
[35] Gueye M, Zighem F, Faurie D, Belmeguenai M and Mercone S 2014 *Appl. Phys. Lett.* **105** 052411
[36] Gueye M, Zighem F, Belmeguenai M, Gabor M S, Tiusan C and Faurie D 2016 *J. Phys. D: Appl. Phys.* **49** 145003
[37] Belmeguenai M, Tuzcuoglu H, Gabor M, Petrisor T Jr, Tiusan C, Berling D, Zighem F, Chauveau T, Chérif S and Moch P 2013 *Phys. Rev.* B **87** 184431
[38] Zighem F, Faurie D, Mercone S, Belmeguenai M and Haddadi H 2013 *J. Appl. Phys.* **114** 073902